Electronic Supplementary Information for

An *in-situ* exsolved Cu-based electrocatalyst from intermetallic Cu$_5$Si compound for efficient CH$_4$ electrosynthesis

Huanhuan Tao,[a,b,c] Fang Wang, [a,b,c] Zhengguo Zhang [a,b,c] and Shixiong Min[* a,b,c]

[a]*School of Chemistry and Chemical Engineering, North Minzu University, Yinchuan, 750021, P. R. China.*

[b]*Key Laboratory of Chemical Engineering and Technology, State Ethnic Affairs Commission, North Minzu University, Yinchuan, 750021, P. R. China*

[c]*Ningxia Key Laboratory of Solar Chemical Conversion Technology, North Minzu University, Yinchuan 750021, P. R. China*

*Corresponding authors: sxmin@nun.edu.cn

1. Experimental

1.1 Chemicals and reagents

All chemicals were of analytical grade and used without further purification. Copper silicide (Cu_5Si, 99.5%), potassium hydroxide (KOH, 90%) and copper oxide (CuO, 99.5%) were purchased from Shanghai Titan Scientific Co., Ltd. Copper power (Cu, 99.9%) was obtained from Zhongmai Metal Materials Co., Ltd. Nafion (5% in lower aliphatic alcohols and water) was purchased from Sigma Aldrich Co., Ltd. Isopropanol ((CH_3)$_2$CHOH, 99.7%) was obtained from Tianjin Damao Chemical Co., Ltd. The high-purity CO_2 (99.999%) was purchased from Jinghua Industrial Gas Co., Ltd. Ultrapure water (18.2 MΩ cm) was obtained from a water purification system (Hitech ECO-S15).

1.2 Synthesis of catalysts

The e-Cu_5Si catalysts were prepared by directly calcining Cu_5Si in air at a desirable temperature ranging from 400~800 ^{o}C for varied amounts of time (1~12 h) with a ramping rate 5° min^{-1}. For comparison, a mixture of Cu_5Si (0.53 g), CuO (0.42 g), and Cu power (0.05 g) was ball-milled (300 r min^{-1}) for 1 h to obtain the physically mixed Cu_5Si/Cu/CuO catalyst. In addition, the as-prepared e-Cu_5Si catalyst was respectively washed with HCl (0.3 M) and $FeCl_3$ (0.3 M) for 8 h and resulting sample were denoted as e-Cu_5Si-HCl and e-Cu_5Si-$FeCl_3$.

1.3 Electrochemical measurements

In order to prepare the cathode electrode, the catalyst slurry was first prepared by dispersing 20 mg of catalyst in a mixed solution containing 1 mL of deionized water, 1 mL of isopropanol, and 25 μL of Nafion ionomer solution with the aid of ultrasonication for 30 min. Then, 1 mL of homogenous catalyst slurry was slowly sprayed on a gas-diffusion layer (GDL) (Avcarb, GDS3250) at 80 °C to achieve a catalyst loading of

~1.7 mg cm^{-2}. The electrochemical CO_2 reduction experiments were performed in a flow cell (Gaoss union,101017-1.2) with a CS350M electrochemical workstation (Corrtest Instruments, Inc., Wuhan). A Ni foam and a saturated Ag/AgCl were used as the anode and reference electrode, respectively, which were separated by anion exchange membrane (Fumasep-FAA-3-PK-130). A 1.0 M KOH aqueous solution was utilized as electrolyte and pumped into cathode chamber at a flow rate of 7.5 mL min^{-1}. CO_2 was fed into cathode chamber at a flow rate of 30 mL min^{-1}.[1] Unless otherwise specified, all the applied potentials were reported as revisable hydrogen electrode (RHE) potentials scale using E (*vs.* RHE)=E (*vs.* Ag/AgCl)+1.023 V–IR_s. For the bulk CO_2 electrolysis, the cathodic compartment was purged with CO_2 (99.999%) at a constant rate of 30 mL min^{-1}. The gas effluent from the cathodic compartment was delivered directly to the sampling loop of an on-line pre-calibrated gas chromatograph (PANNA GC-A91 plus) equipped with a thermal conductivity detector (TCD) and a flame ionization detector (FID). Faradaic efficiency (FE) of gaseous products at each applied potential was calculated based on following equation:

$$FE_i = \frac{Z_i \times G \times V_i \times t \times p_0 \times F \times 10^{-3}}{Q_{total} \times R \times T_0} \times 100\%$$

where Z is the number of electrons transferred; G is volumetric outlet flow rate (27.6 mL min^{-1}); V_i is the volume ratio of gas product i; t is reaction time (min); P_0 and T_0 are atmospheric pressure (101.3 KPa) and reaction temperature (298.15 K); respectively. F is faradaic constant (96485 C mol^{-1}); Q_{total} is integrated charge at each applied potential and R is ideal gas constant (8.314 J·mol^{-1} K^{-1}).

At the end of the electrolysis, the produced liquid phase products were detected by using a high-performance liquid chromatography (HPLC, Hitachi) system equipped with C18 column and UV detector.

The solution resistance (R_s) was determined by electrochemical impedance spectroscopy (EIS) measurements, which were performed in a frequency range from 0.01 Hz to 100 kHz at a voltage amplitude of 5 mV.

The electrochemical surface area (ECSA) of the electrodes was determined by measuring the electric double layer capacitance (C_{dl}). Cyclic voltammetry (CV) tests were performed at different scan rates in a N_2 bubbling 0.1 M $KHCO_3$ electrolyte. The potential window of CV is selected between 0.84~0.94 V, where only double-layer charge and discharge are related. The total charging current at a scan rate of 10-100 mV s^{-1} was determined to be the difference between the anode current and the cathode current at 0.85 V. These capacitive currents are plotted against the scan rate, and the slope of the plot is divided by 2 to obtain the value of C_{dl}.[2]

1.4 Characterizations

Powder X-ray diffraction (PXRD) patterns were investigated with a Rigaku smartlab diffractometer with a nickel filtrated Cu $K\alpha$ radiation in the 2θ range of 5~80° with a scanning rate of 5° min^{-1}. *In-situ* high temperature XRD (*in-situ* HTXRD) measurements were carried out with a Panalytical Empyrean XRD diffractometer at a standard Bragg-Brentano reflection geometry in the 2θ range of 30°~80° with a nickel filtrated Cu $K\alpha$ radiation with a scanning rate of 5° min^{-1}. During the measurements, the sample was annealed in in air at a ramping rate of 5° min^{-1} to a desired temperature for 10 min. Scanning electron microscopy (SEM) images were taken with a ZEISS EVO 10 scanning electron microscope. Transmission electron microscopy (TEM) images were taken with a FEI Talos F200x field emission transmission electron microscope. HAADF-STEM observations of the samples were performed on a Titan Cubed Themis G^2 300 STEM. X-ray photoelectron spectroscopy (XPS) measurements of the samples were performed on a ThermoFisher Escalab-250Xi electron

spectrometer using an Al $K\alpha$ X-ray source. Binding energies were referenced to the C 1s peak (set at 284.8 eV) of the sp^2 hybridized (C=C) carbon from the sample. *In-situ* Raman experiments were performed using a HORIBA HR Evolution Raman microscope in a flow cell (Gaoss union, C031-3) with a water immersion objective. During testing, CO_2 with a constant flow rate of 30 mL min^{-1} flowed through the gas compartment, whereas 1 M KOH solution with a flow rate of 7.5 mL min^{-1} flowed through the electrolyte compartment. A Pt wire was used as the counter electrode, and a 785 nm laser was used for Raman testing. Signals were recorded using a 5 s integration and averaging 10 scans.[3] The temperature-programmed desorption of NH_3 (NH_3-TPD) and CO_2 (CO_2-TPD) were performed using a chemisorption analyzer (Micromeritics Autochem II 2920) equipped with a TCD detector. A100 mg sample was heated from room temperature to 400 °C at a ramping rate of 10 °C min^{-1} and held at 400 °C for 1 h, followed by cooling to 50 °C at a heating rate of 10 °C min^{-1} under high-purity Ar gas. After that, the carrier gas was switched to 10% NH_3 (He balanced) or CO_2 (30 mL min^{-1}) and held on 120 min. Subsequently, the physically adsorbed NH_3 or CO_2 on the sample was purged with He gas (30 mL min^{-1}) for 1 h. Finally, the sample was heated from 50 °C to 700 °C at a ramping rate of 10 °C min^{-1}.
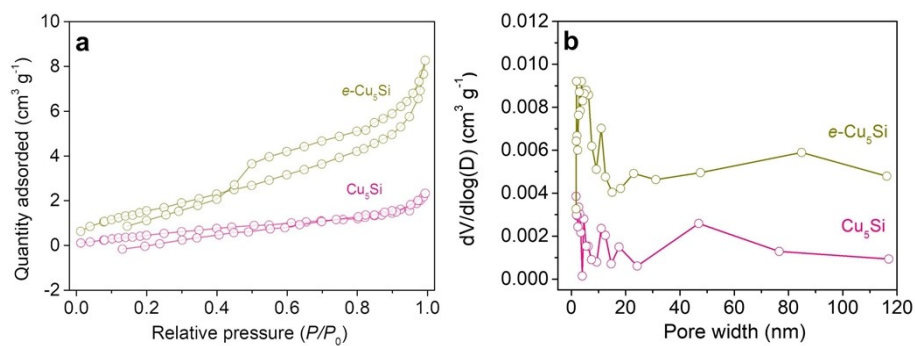
2. Additional data
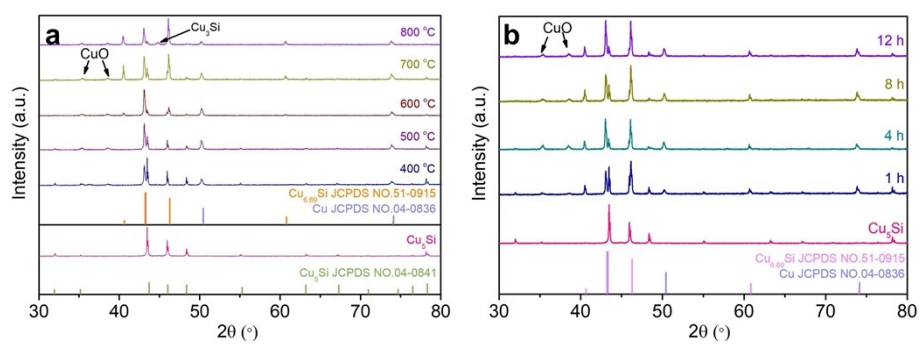
Fig. S1 PXRD patterns of *e*-Cu$_5$Si prepared at (a) different air-annealing temperatures (Time: 8 h) and (b) times (Temperature: 700 °C).
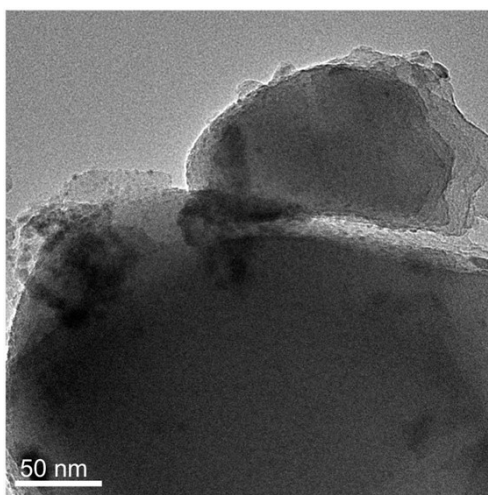
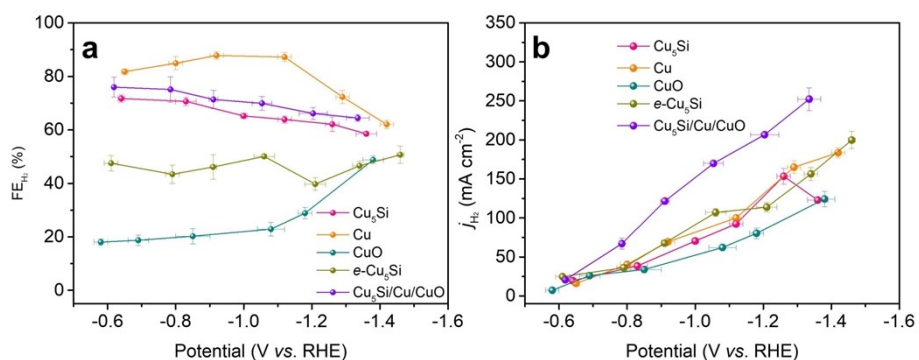**Fig. S2** TEM image of *e*-Cu$_5$Si catalyst.
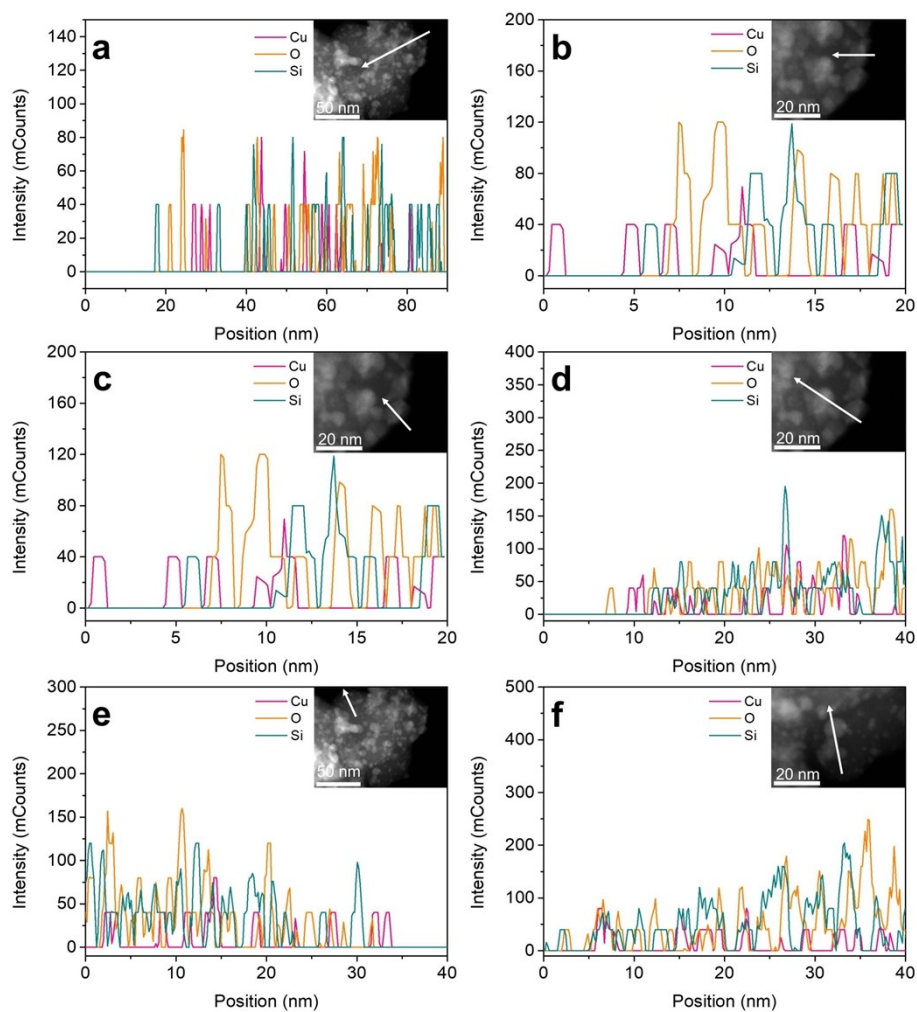
**Fig. S3** EDX line scans on randomly selected positions on e-Cu$_5$Si catalyst.

Fig. S4 (a) N$_2$ adsorption-desorption isotherms and (b) pore size distributions of

pristine Cu$_5$Si and e-Cu$_5$Si.

Table S1 Textural properties of pristine Cu$_5$Si and e-Cu$_5$Si catalysts.

Catalyst	S_{BET}(m^2 g^{-1})	Pore diameter (nm)
e-Cu$_5$Si	6.3	4.9
Cu$_5$Si	2.4	5.8

Fig. S5 (a) FEs and (b) partial current densities for H$_2$ production over e-Cu$_5$Si, pristine Cu$_5$Si, unsupported Cu and CuO, and Cu$_5$Si/Cu/CuO.
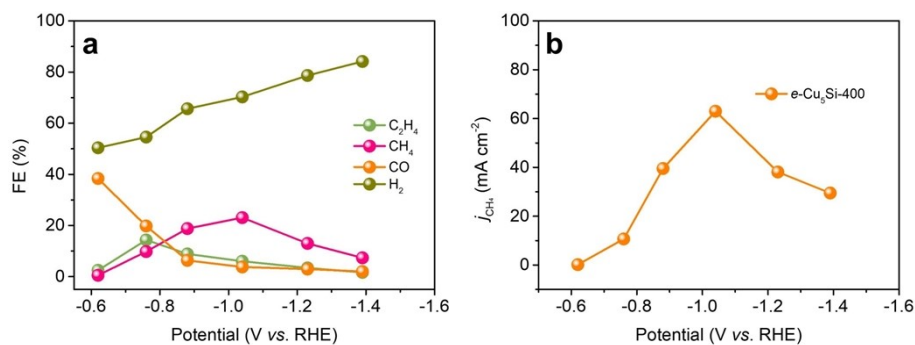
Fig. S6 (a) FEs of CO$_2$ reduction products and (b) partial current density of CH$_4$ over e-Cu$_5$Si-400 as a function of applied potentials.
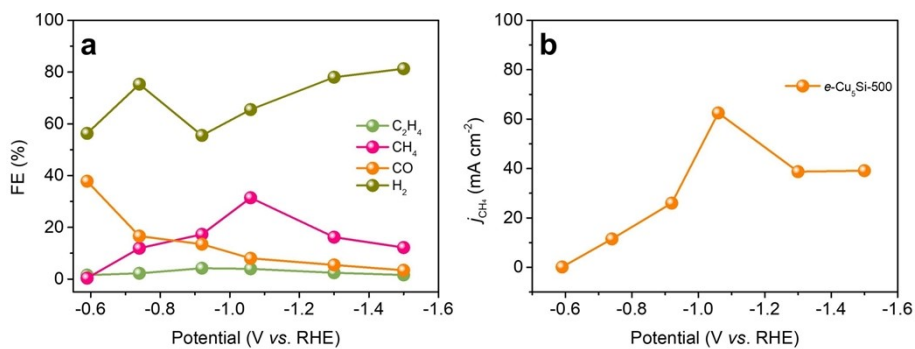
Fig. S7 (a) FEs of CO_2 reduction products and (b) partial current density of CH_4 over

e-Cu$_5$Si-500 as a function of applied potentials.
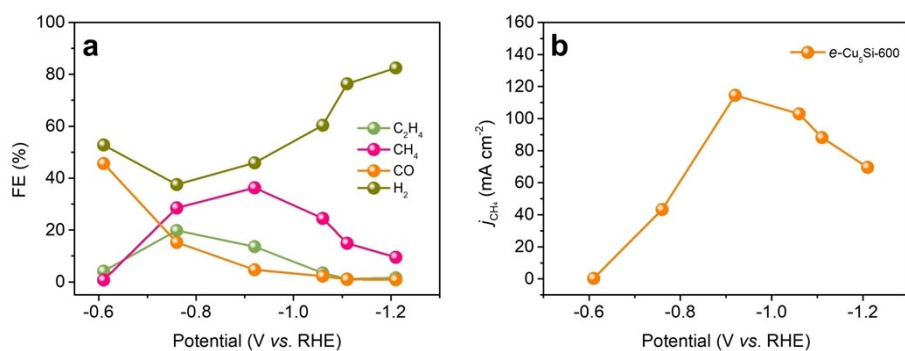
Fig. S8 (a) FEs of CO_2 reduction products and (b) partial current density of CH_4 over

e-Cu$_5$Si-600 as a function of applied potentials.
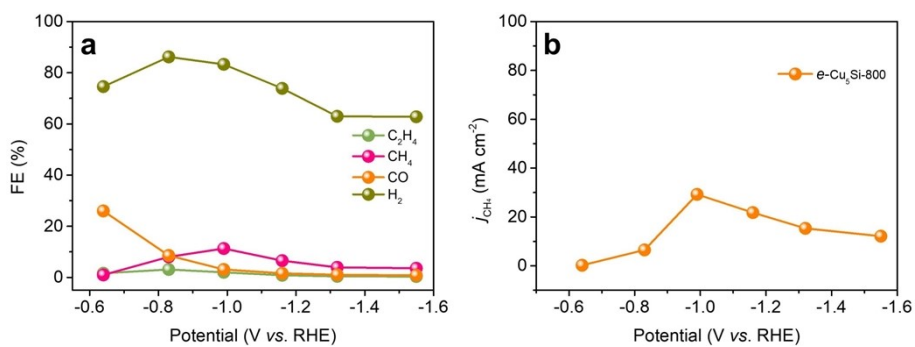
Fig. S9 (a) FEs of CO_2 reduction products and (b) partial current density of CH_4 over

e-Cu$_5$Si-800 as a function of applied potentials.
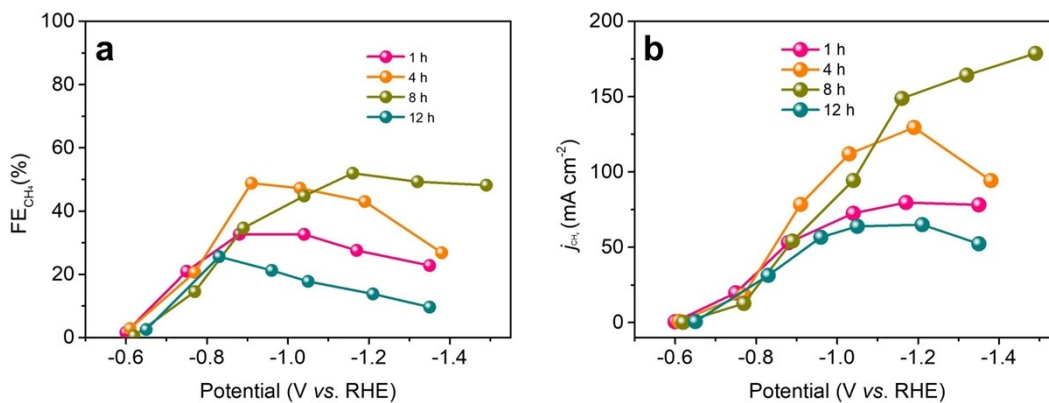
Fig. S10 (a) FEs and (b) partial current densities for CH$_4$ production over e-Cu$_5$Si catalysts prepared at 700 °C for different annealing time.
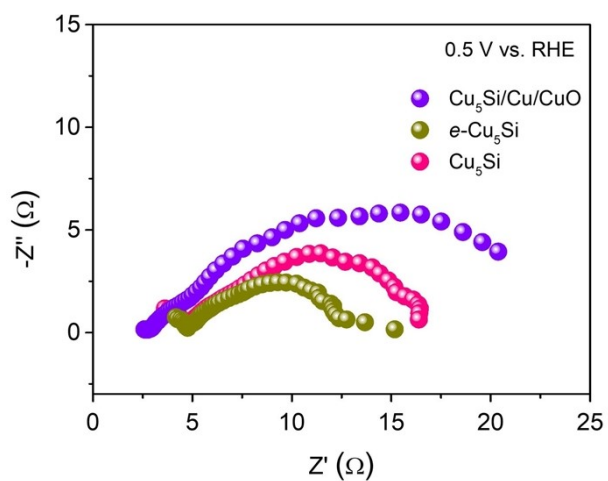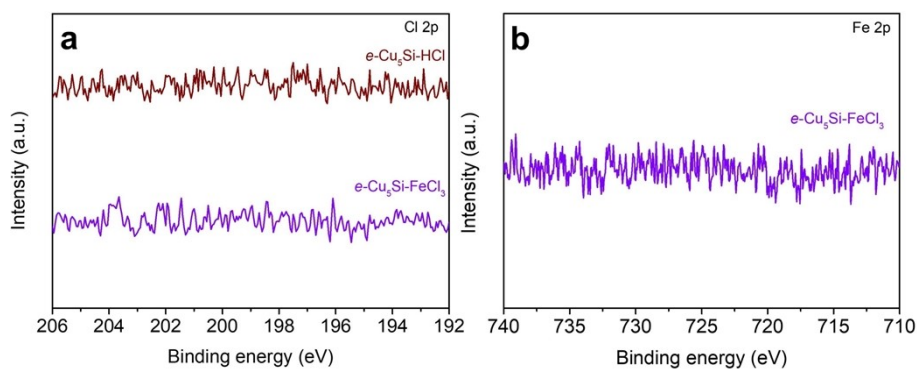

Fig. S11 EIS curves of pristine Cu$_5$Si, e-Cu$_5$Si and Cu$_5$Si/Cu/CuO catalysts obtained.
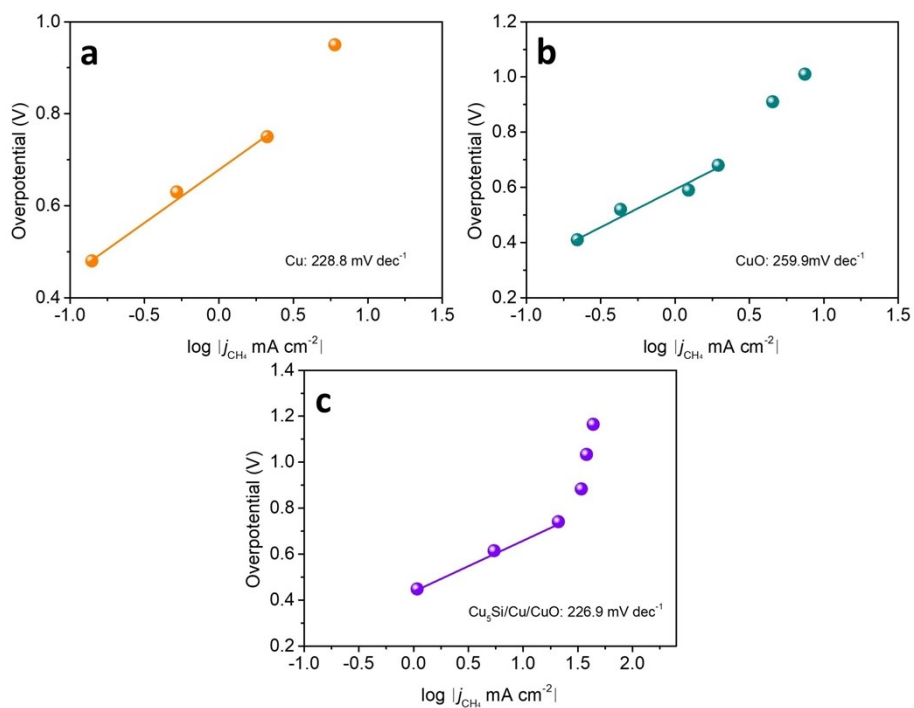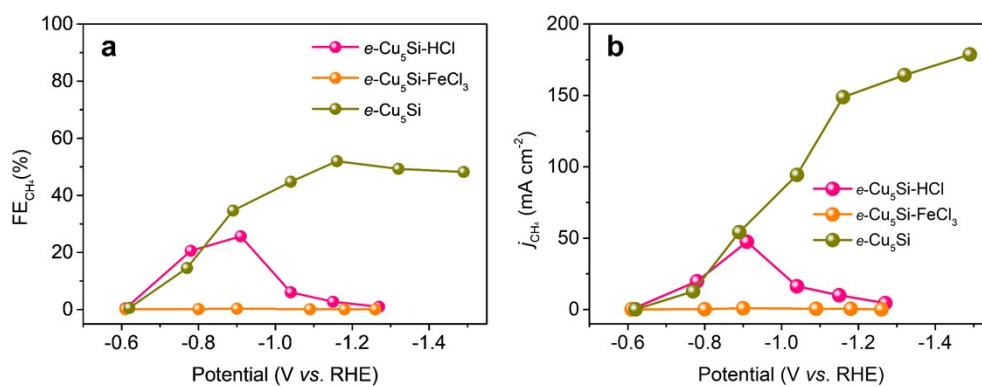
Fig. S12 CH$_4$ partial current density Tafel plots for (a) unsupported Cu, (b) unsupported CuO, and (c) Cu$_5$Si/Cu/CuO catalysts.
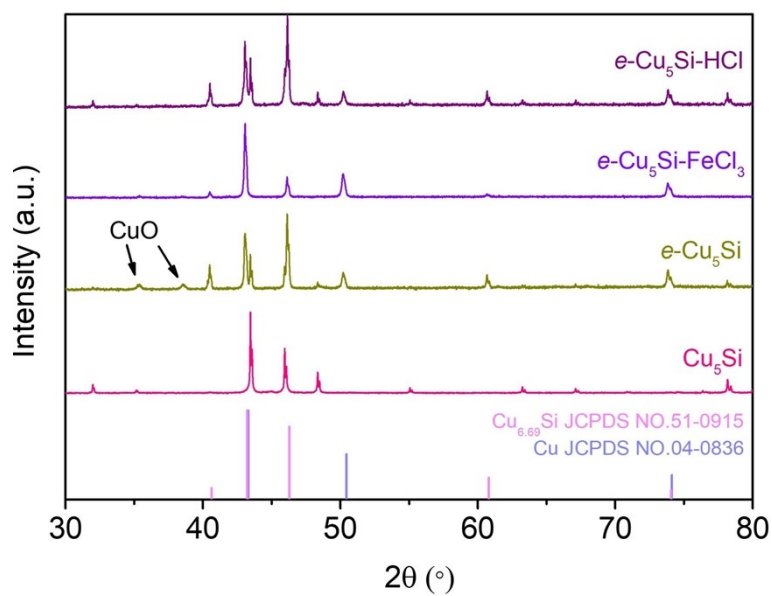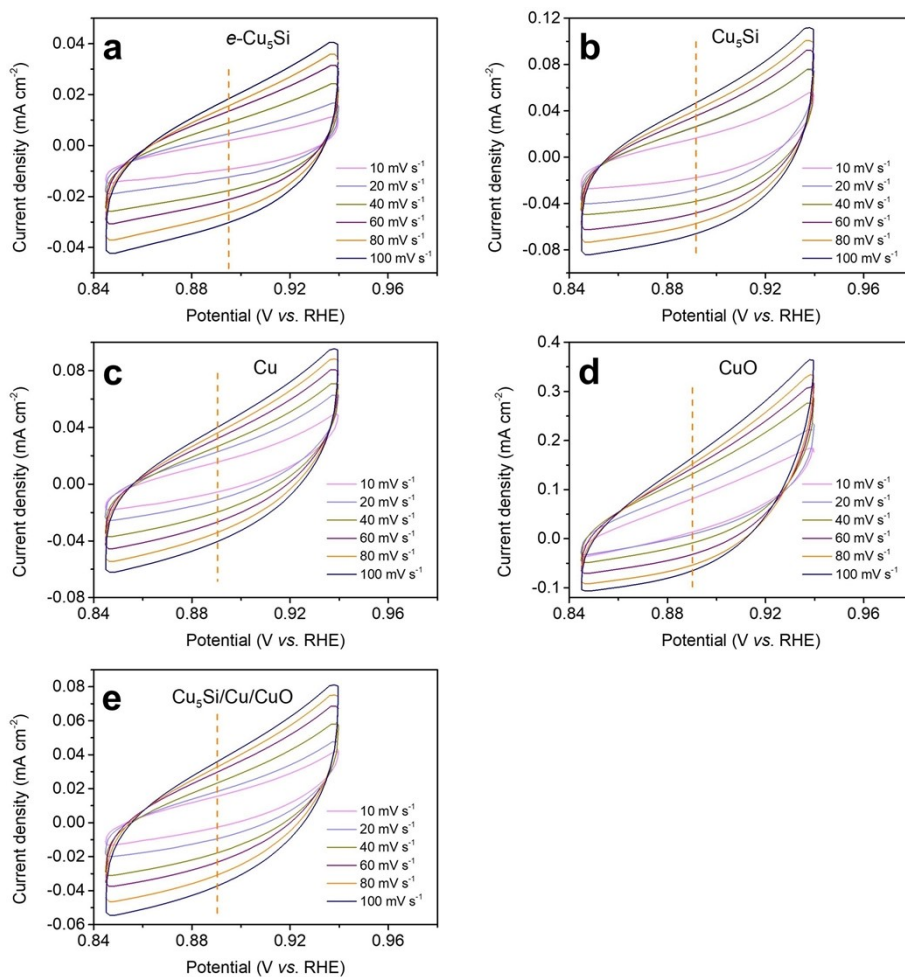

Fig. S13 PXRD patterns of pristine Cu$_5$Si, e-Cu$_5$Si, e-Cu$_5$Si-FeCl$_3$, and e-Cu$_5$Si-HCl.
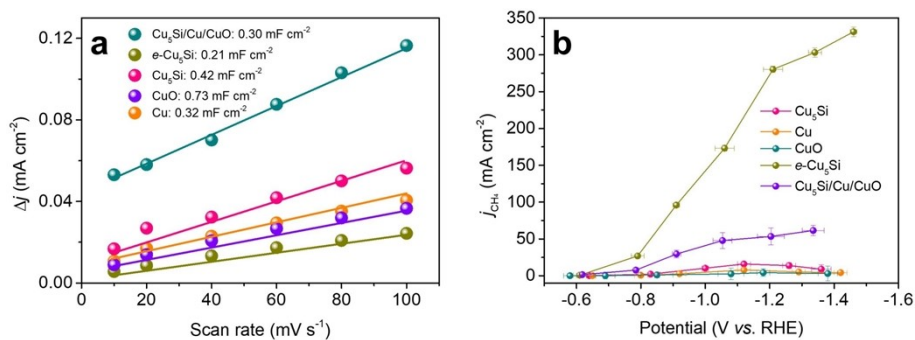
Fig. S14 (a) Cl 2p and (b) Fe 2p XPS spectra of *e*-Cu$_5$Si-FeCl$_3$ and *e*-Cu$_5$Si-HCl.

Fig. S15 (a) FEs and (b) partial current densities for CH$_4$ production over *e*-Cu$_5$Si, *e*-Cu$_5$Si-FeCl$_3$, and *e*-Cu$_5$Si-HCl.

Fig. S16 CV curves at different scan rates in the non-Faradaic capacitance range of (a) e-Cu_5Si, (b) pristine Cu_5Si, (c) unsupported Cu, (d) unsupported CuO, and (e) $Cu_5Si/Cu/CuO$.


Fig. S17 (a) Current density plotted against scan rate of e-Cu_5Si, pristine Cu_5Si, unsupported Cu and CuO, and $Cu_5Si/Cu/CuO$. (b) ECSA-normalized partial current densities of CH_4 production on e-Cu_5Si, pristine Cu_5Si, unsupported Cu and CuO and $Cu_5Si/Cu/CuO$.
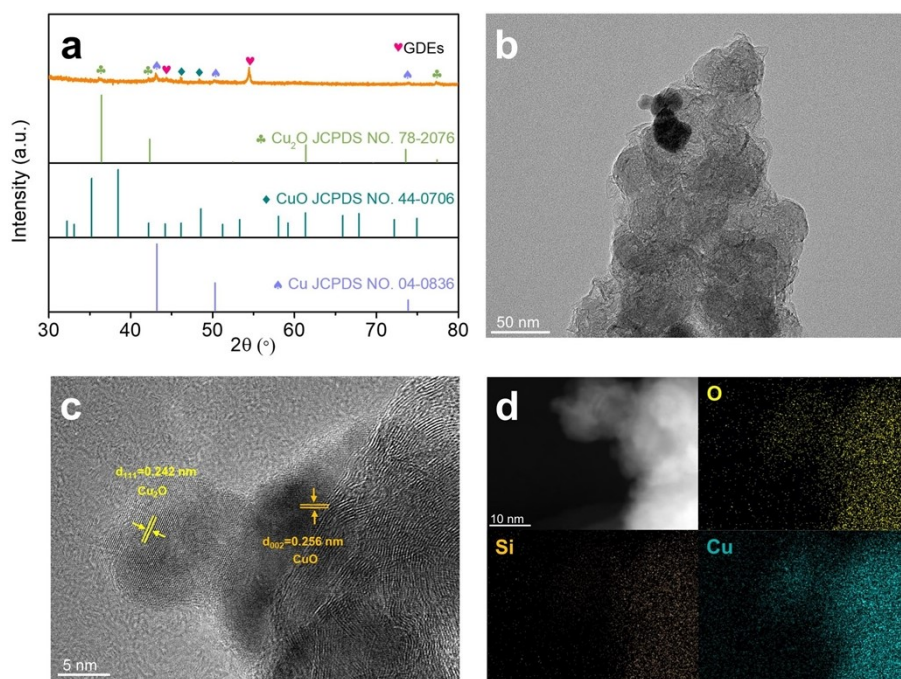
Fig. S18 (a) PXRD pattern, (b) TEM, (c) HRTEM, and (d) HAADF-STEM images and the corresponding EDX elemental mapping images of the e-Cu$_5$Si catalyst after CO$_2$RR stability test.
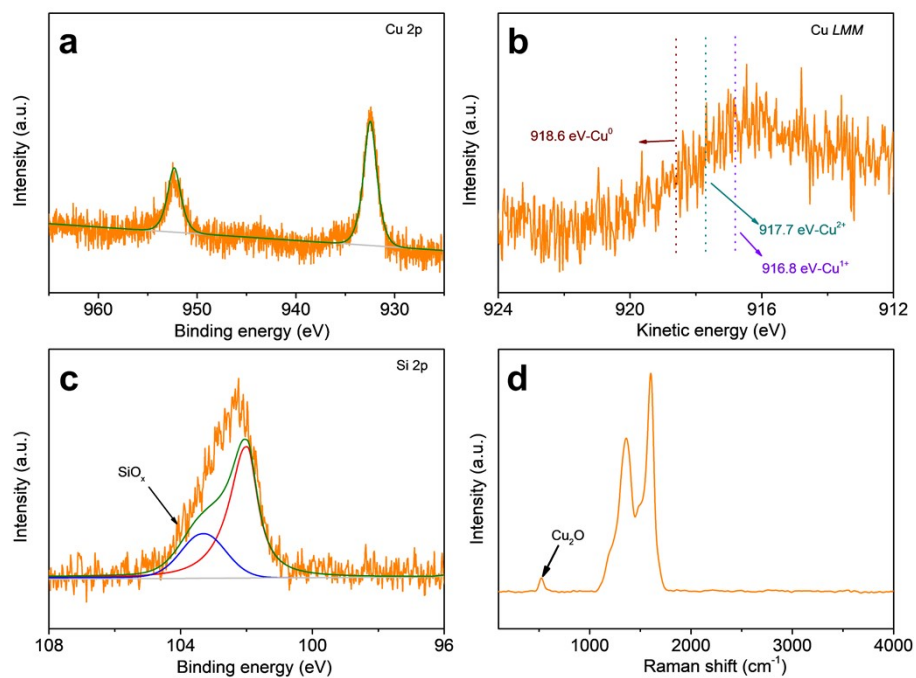
Fig. S19 (a) Cu 2p, (b) Cu *LMM* Auger, (c) Si 2p XPS spectra, and (d) Raman spectrum of e-Cu$_5$Si after CO$_2$RR stability test.
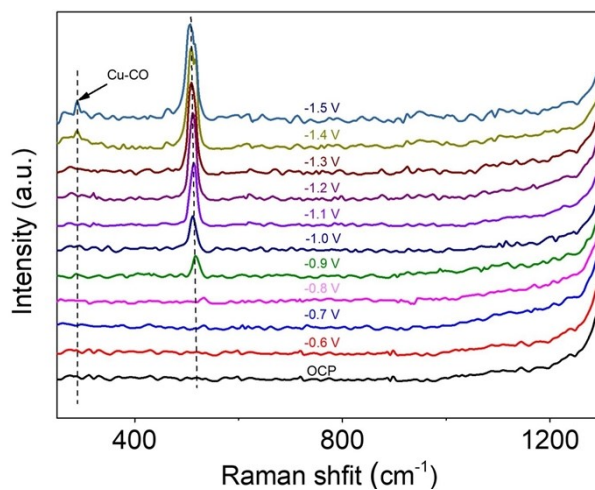
Fig. S20 *In-situ* Raman spectra recorded at various potentials for pristine Cu$_5$Si.

Supplemented references

1. S. Min, H. Chang, H. Tao and F. Wang, *J. Mater. Chem. A*, 2023, **11**, 15643-15650.

2. W. Deng, S. Min, F. Wang, Z. Zhang and C. Kong, *Dalton Trans.*, 2020, **49**, 5434-5439.

3. J. Duan, T. Liu, Y. Zhao, R. Yang, Y. Zhao, W. Wang, Y. Liu, H. Li, Y. Li and T. Zhai, *Nat. Commun.*, 2022, **13**, 2039.